

Environmentally important, poorly crystalline Fe/Mn hydrous oxides: Ferrihydrite and a possibly new vernadite-like mineral from the Clark Fork River Superfund Complex

MICHAEL F. HOCELLA, JR.,^{1,*} TAKESHI KASAMA,^{2,†} ANDREW PUTNIS,² CHRISTINE V. PUTNIS,² AND JOHNNIE N. MOORE³

¹Nanogeoscience and Technology Lab, Department of Geosciences, Virginia Tech, Blacksburg, Virginia 24061-0420, U.S.A.

²Institut für Mineralogie und Interdisciplinary Centre for Electron Microscopy and Microanalysis, Universität Münster, Corrensstrasse 24, D-48149 Münster, Germany

³Department of Geology, University of Montana, Missoula, Montana 59812, U.S.A.

ABSTRACT

Ferrihydrite and a vernadite-like mineral, in samples collected from the riverbeds and floodplains of the river draining the largest mining-contaminated site in the United States (the Clark Fork River Superfund Complex), have been studied with transmission electron microscopy (TEM) and energy dispersive X-ray (EDX) analysis. These poorly crystalline minerals are environmentally important in this system because contaminant heavy metals (As, Cu, Pb, and/or Zn) are always associated with them. Both two- and six-line ferrihydrite have been identified with selected-area electron diffraction. For the vernadite-like mineral, the two *d* values observed are approximately between 0.1 and 0.2 Å larger than those reported for vernadite, the Mn hydrous oxide that is thought to have a birnessite-like structure, but which is disordered in the layer stacking direction. In several field specimens, the ferrihydrite and vernadite-like minerals are intimately mixed on the nanoscale, but they also occur separately. It is suggested that the vernadite-like mineral, found separately, is produced biogenically by Mn-oxidizing bacteria, whereas the same mineral associated with ferrihydrite is produced abiotically via the heterogeneous oxidation of Mn_{aq}^{2+} initially on ferrihydrite surfaces. Evidence from this study demonstrates that the vernadite-like mineral sorbs considerably more toxic metals than does ferrihydrite, demonstrating that it may be a good candidate for application to heavy-metal sorption in permeable reactive barriers.

INTRODUCTION

Environmental aspects of mineralogy encompass extraordinarily diverse subjects that are vitally important in several Earth sustainability issues (see, e.g., Banfield and Nealson 1997; Buseck et al. 2000; Hochella 2002). One such issue is the short- and long-term effects of mine wastes on the environment. Certainly, metals gained from the world's mining industries are vital to all of us, but not without incurring an environmental price. Present and former mining sites, numbering in the hundreds of thousands the world over, release acid and metals into the surrounding environment when sulfides are involved (Moore and Luoma 1990). Metal release can occur and propagate as much as hundreds of kilometers down hydrologic gradient from the mining and mine-waste sites for months, years, or even decades to centuries. In the United States alone, 20 000 km of streams and rivers have been adversely affected by mining operations (DaRosa and Lyons 1997). Understanding these systems has become an important part of environmental mineralogy and geochemistry (e.g., Jambor and Blowes 1994; Alpers and Blowes 1994; Jambor et al. 2003).

The mineralogy, water chemistry, and microbiology of mining and smelter wastes dictate the attenuation or release of toxic metals from any particular site, whether the wastes are in a tailings impoundment at the mine site or as river sediment hundreds of kilometers away. Within this construct, toxic metal association/transport and bioavailability then becomes the central issue. In terms of mineralogy, it is common in many mining waste scenarios for the formation of secondary minerals to be influenced by high solute concentrations of iron at low pH from the dissolution of pyrite and other Fe-containing sulfides. Mixing with oxygenated surface waters results in the formation of iron oxyhydroxides and hydrous oxides, such as goethite, lepidocrocite, and ferrihydrite, as well as hydroxysulfates such as schwertmannite and jarosite (e.g., Alpers et al. 1994; Schwertmann et al. 1995; Jambor and Blowes 1998). Although manganese is usually much less abundant, various manganese (hydr)oxides and hydrous oxides have also been observed (e.g., Lind and Hem 1993; Davis et al. 1993; Hudson-Edwards et al. 1996; Holmström and Öhlander 2001).

This article is part of a larger study in which we have assessed, using principally transmission electron microscopy (TEM) and electron diffraction, coupled with energy dispersive X-ray (EDX) analysis, the distribution and bioavailability of toxic heavy metals from mining-contaminated floodplains and riverbeds in and along Silver Bow Creek and the Clark Fork River, Montana, USA (Fig.

* E-mail: hochella@vt.edu

† Present address: Department of Materials Science and Metallurgy, University of Cambridge, Pembroke Street, Cambridge CB2 3QZ, U.K.

1; Hochella et al. 2005). These waterways are a major and critical part of the largest “Superfund site” in the United States, the Clark Fork River Superfund Complex (Moore and Luoma 1990). This site has been affected by nearly 150 years of large-scale base-metal mining operations and has the characteristics of mine-waste sites described above. In this article, for several reasons we have concentrated on the poorly crystalline Fe- and Mn-hydrous oxides found in these floodplain and riverbed samples. First, one hydrous oxide described here is a vernadite-like mineral (nominally $MnO_2 \cdot nH_2O$ with small amounts of alkali, alkaline-earth, and transition metals present) that to our knowledge has never been described before. It has a very high affinity for toxic metals in this system, even more so than ferrihydrite. Second, this mineral and ferrihydrite (nominally $5Fe_2O_3 \cdot 9H_2O$), which as described below can be intermixed on the nanometer scale, can easily be overlooked in studies of these types of samples. The minerals cannot be positively identified optically, and are not in high enough concentrations to be identified using powder X-ray diffraction, especially because their diffraction maxima are so broad and weak. The TEM is essential for finding and characterizing them. Third, these are the only secondary minerals that are consistently associated with toxic metals, and they are some of the most important phases in the take-up and release of these metals in large portions of this superfund complex.

SAMPLES AND METHODS

Sampling locations and sample designation

Samples from this study come from two locations, the first on Silver Bow Creek at a location called Miles Crossing, about 1.5 km from the Ramsey Exit off Interstate 90 and 8 km west of Butte, Montana, U.S.A. (Fig. 1). This stream drains the mining areas in and around Butte. A sample was collected near the stream edge where the water depth was about 15 cm. This sample, designated MC-riverbed (equivalent to MC-4 in Hochella et al. 2005), is a black mud that was overlain by a thin veneer of uppermost riverbed, a light-brown coarser sediment less than 1 cm thick.

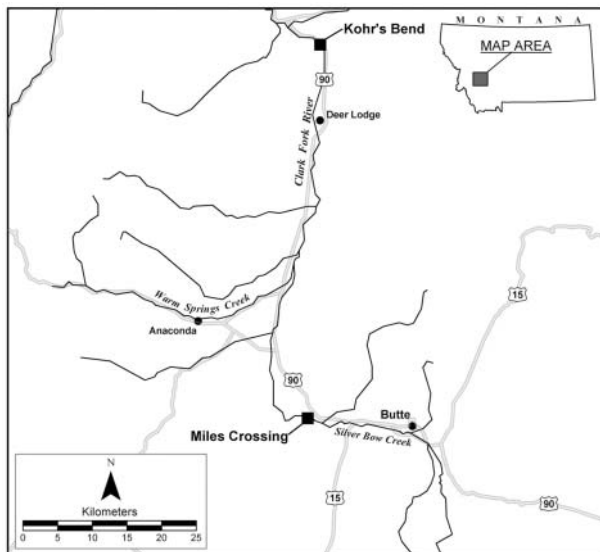


FIGURE 1. Map of the Butte, Anaconda, and Clark Fork River headwaters area of Montana, U.S.A. The state outline is shown in the upper right with a box indicating the position of the map area. The Miles Crossing and Kohr's Bend sampling locations, described in the text, are shown.

A second group of samples was collected 80 river kilometers downstream from Miles Crossing and well beyond the confluence of several streams that form the Clark Fork River. This river drains the entire Butte-Anaconda area, which includes all historic mining areas and the massive tailings and smelter waste piles in the region. This particular collecting location is known as Kohr's Bend and is just off Interstate 90 at the Beck Hill exit (Fig. 1). Three samples from this location are included in this study. The first, which looks like sample MC-riverbed described above, was also collected from the riverbed near its edge and is designated KB-riverbed. Digging into the edge of the cutbank at this location with a trowel revealed two distinct levels of floodplain sediment, both originating from mine tailings and smelter wastes. In this study, one sample (designated KB-floodplain1, equivalent to KB-1 in Hochella et al. 2005) was taken at a depth of 15 cm from the level forming the present floodplain surface. The second (designated KB-floodplain2, equivalent to KB-2 in Hochella et al. 2005) was collected from the second, deeper layer at a depth of 30 cm. All of the samples described above were placed in plastic tubs and were allowed to completely dry in air over the next several days before capping for storage.

Transmission electron microscopy

TEM ultramicrotomed thin sections were prepared in a similar fashion to the method described in Hochella et al. (1999), with an updated description in Hochella et al. (2005). Briefly, each sample was dispersed with light grinding. A series of dry and wet sieving was used to obtain the $< 25 \mu\text{m}$ fraction. A final light grinding was performed to continue to disperse the samples as much as possible. The samples were then impregnated with epoxy, thinned by polishing to a thickness of 10 to $20 \mu\text{m}$, and finally cemented into an epoxy block for ultramicrotome cutting with a diamond knife as described in Hochella et al. (1999). Final cut sections for this study were between 20 and 50 nm thick. The resulting films, floating on water in the trough of the diamond knife holder, were recovered on 300 mesh nickel TEM grids. Finally, the grids holding the sections were lightly coated with carbon.

Ultramicrotomed sections were loaded onto nickel grids and studied with a JEM-3010 (JEOL) TEM operated with a LaB₆ filament. We used a double-tilting, analytical specimen holder (beryllium components) for observation. All imaging, diffraction, and analyses were performed at a beam energy of 300 kV and beam currents between 115 and 119 nA.

An Oxford Link ISIS system equipped with an atmosphere thin-window was used for EDX analysis in the JEOL 3010. Semi-quantitative determination of key metal-concentration ratios were performed using the Cliff-Lorimer ratio technique and k_{AB} -factors published in Williams and Carter (1996) and references therein.

Under the beam conditions noted above, beam damage was not observed for any of the Fe- and Mn-hydrous oxides observed in this study. Still, care was taken to limit beam exposure, and to collect image, diffraction, and EDX information quickly. Sample degradation was monitored by diffraction-pattern quality and EDX-measured compositional changes with time. All data and images in this article are free of degradation artifacts.

The precise measurement of d values from diffuse electron diffraction rings is critical in this study. Camera constants for the TEM at different camera lengths were carefully calculated from diffraction patterns of gold films. All electron diffraction patterns were collected under optimum focus conditions, or very slightly underfocused conditions, at camera lengths of either 100 or 150 cm. Measurement of d values of well-crystallized minerals in our ultrathin sections were within $\pm 0.05 \text{ \AA}$ or less of that reported for the mineral (for d values below approximately 3 \AA). When measuring d values of the diffuse diffraction rings of ferrihydrite and the Mn-rich hydrous oxides observed in this study, the ring radius was carefully measured from several patterns to the center of the diffuse ring. These measurements were highly reproducible, and should have an error of no more than, and probably less than, $\pm 0.05 \text{ \AA}$.

RESULTS

The ferrihydrite and vernadite-like minerals observed in this study are listed in Table 1 along with the corresponding photomicrographs for each (Figs. 2–7). These minerals probably make up no more than a few percent or less of the field samples judging from how often they were observed in the TEM and from their absence in powder XRD patterns of the bulk sample. However, these minerals were observed in the riverbed samples from both Miles Crossing and Kohr's Bend, and in both of the floodplain samples originating from mine tailings/smelter wastes at Kohr's

Bend. Three of the five observations, including MC-riverbed shown in Figure 2, KB-floodplain1 shown in Figure 3, and one of the two minerals of interest observed in KB-floodplain2 shown in Figure 4, can be easily classified as ferrihydrite, although there are a few additional points of interest. First, only sample KB-floodplain2 (Fig. 4) contains no detectable Mn, whereas in the other two, MC-riverbed (Fig. 2) and KB-floodplain1 (Fig. 3), the atomic ratio of Fe to Mn is approximately 9:1. Second, two of these three (one each from the two floodplain beds sampled at Kahr's Bend; Figs. 3 and 4) are two-line ferrihydrite with broad, weak diffraction rings at 2.55 and 1.50 Å. The third sample, from

the riverbed at Miles Crossing (Fig. 2), is probably a six-line ferrihydrite. The diffraction pattern has broad, weak diffraction rings at 2.57, 2.20, 1.70, and 1.49 Å. The other two lines of six-line ferrihydrite should be at about 1.99 and 1.55 Å, but are not visible in this pattern. This is because the 1.99 Å line is commonly the weakest in six-line ferrihydrite patterns, and the 1.55 Å line is a weak peak on the shoulder of the 1.49 Å line. Therefore, it is not surprising that the 1.99 and 1.55 Å lines are not observed

TABLE 1. Fe/Mn hydrous oxides observed in this study

Sample*	Composition†	Obs. <i>d</i> values (Å)‡			Sorbed metals§	Fig.
MC-riverbed	Fe ₉₀ Mn ₁₀	2.57	2.20	1.70	1.49 1.20	Zn, Astr 2
KB-floodplain1	Fe ₉₀ Mn ₁₀	2.55	2.10	—	1.50 1.20	Pb, As, Zn ^{tr} 3
KB-floodplain2	Fe ₁₀₀ Mn ₀	2.55	2.10	—	1.50 1.20	Cu, Pb, As ^{tr} 4
KB-floodplain2	Fe ₆₀ Mn ₄₀	2.66	2.13	—	1.54 1.20	Pb, Cu, Zn, As 5
KB-riverbed	Fe ₉₂ Mn ₁₀₀	2.67	2.13	—	1.59 1.20	Zn, As ^{tr} , Pb ^{tr} 6,7

* See section entitled "Sampling locations and sample designation" for an explanation of this column.

† The relative amounts of Fe to Mn in the Fe/Mn hydrous oxides are listed here.

‡ In all cases, there was very weak diffraction at 2.1–2.2 Å and 1.2 Å from the epoxy film/carbon film holding the sample. Possibly some or most of the diffraction intensity at these positions was also contributed by the mineral samples, especially in the range of 2.1–2.2 Å. See text for further information.

§ Sorbed metals are given in the order of decreasing abundance. Cu:(Fe + Mn) and Zn:(Fe + Mn) ratios are as high as 5:100, As:(Fe + Mn) ratios as high as 2:100, and Pb:(Fe + Mn) as high as 0.2:100. "tr" means trace, and indicates that the EDX peak was just above background, i.e., near the detection limit for this technique.

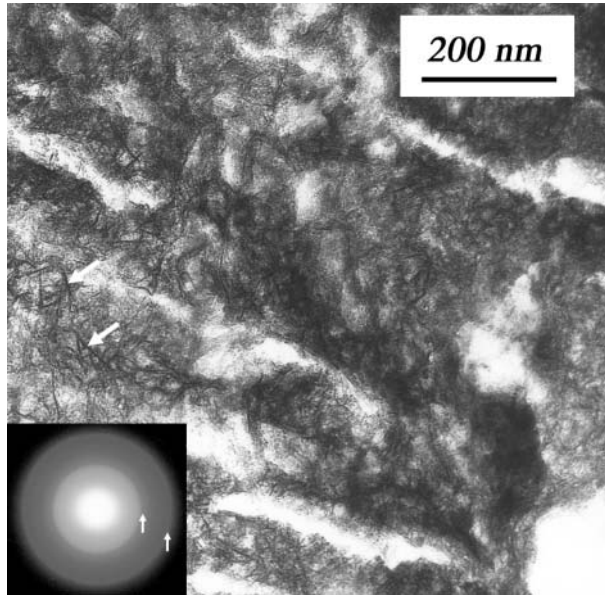


FIGURE 2. TEM image of six-line ferrihydrite with a small amount of a vernadite-like mineral (dark, fiber-like particles, two of which are indicated by white arrows in the image) from the riverbed at Miles Crossing. The selected-area diffraction pattern of the ferrihydrite shows the broad, very weak lines from this mineral. The inner and outer arrows indicate the positions of the 2.57 and 1.49 Å lines, respectively. The 2.20 and 1.70 Å lines are barely visible between these two, and are most easily seen on the left side of center.

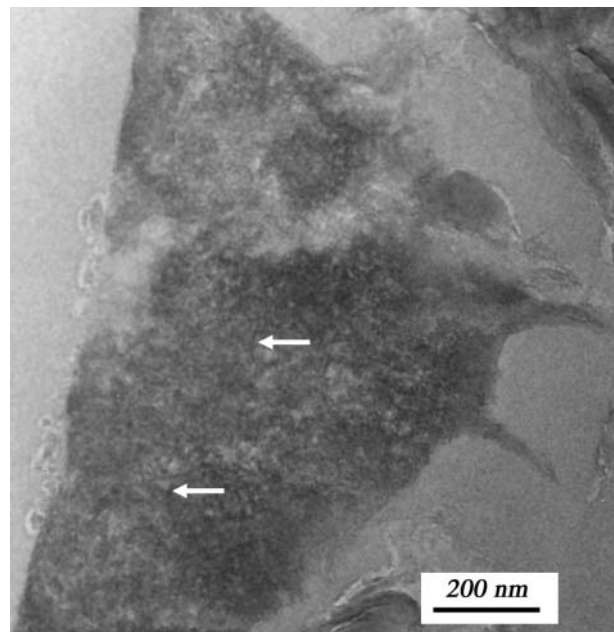


FIGURE 3. TEM image of a two-line ferrihydrite with a small amount of a vernadite-like mineral from the upper level of the floodplain at Kahr's Bend, collected at a depth of 15 cm. The arrows point to rare fiber-like features in this image.

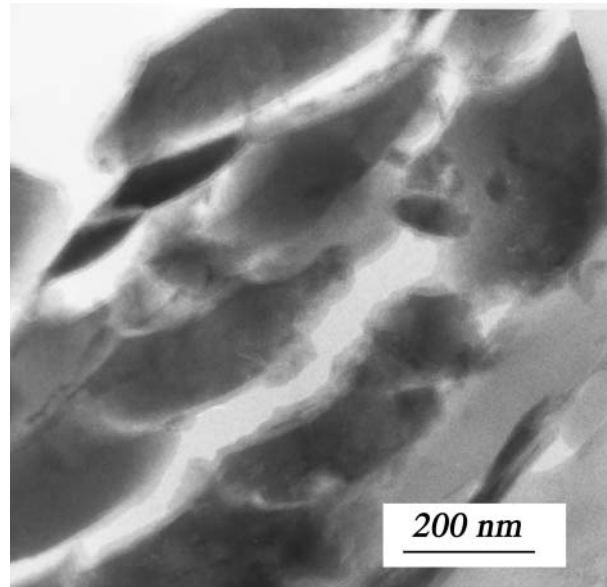


FIGURE 4. TEM image of smooth-textured two-line ferrihydrite from the lower layer sampled in the floodplain at Kahr's Bend, collected from a depth of about 30 cm. Everything in the image is ferrihydrite.

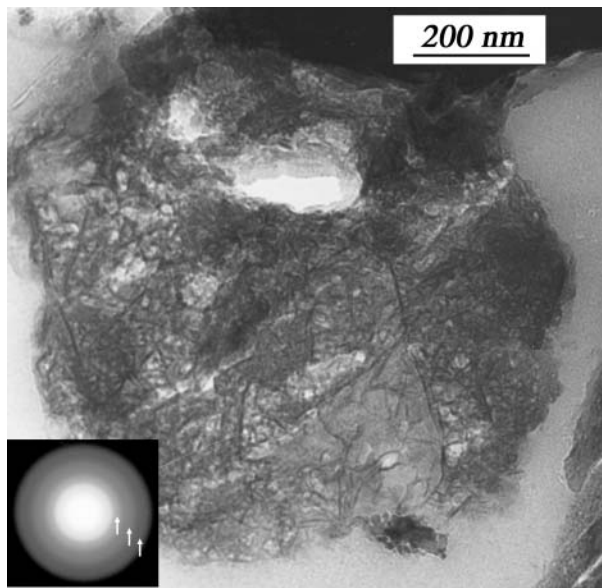


FIGURE 5. TEM image of a mixture of two-line ferrihydrite and the vernadite-like mineral of roughly equal proportions collected from the lower layer in the floodplain at Kohr's Bend. The diffraction bands are even broader than, for example, those from ferrihydrite shown in Figure 2 because they result from the overlap of the broad diffraction bands of these two minerals (the inner arrow points to the combination of diffraction bands from the two minerals at about 2.55 and 2.67 Å; the outer arrow points to the combination of diffraction bands from the two minerals at about 1.50 and 1.59 Å). The middle arrow points to one of the broad diffraction bands from the epoxy/carbon film holding the specimen.

in our patterns of MC-riverbed. In summary, all diffraction-line positions observed for two- and six-line ferrihydrite in this study are fully consistent with the electron diffraction observations and *d* values seen in previous studies of these minerals (see Janney et al. 2000, and references therein).

The other two observations made in this study and noted in Table 1 are not so easily classified. One observation, also from the lower bed of mine tailings on the floodplain at Kohr's Bend (KB-floodplain2; Fig. 5), is that the sample has an EDX-measured Fe:Mn atomic ratio of approximately 3:2. Only two diffraction maxima, at 2.66 and 1.54 Å, can be assigned to this mineral because the weak diffraction lines from the epoxy/carbon film are at 2.1 and 1.2 Å. The line at 2.66 Å is significantly larger than the 2.55 Å line observed for two-line ferrihydrite. The other observation is that a mineral in the sample from the riverbed at Kohr's Bend (KB-riverbed; Fig. 6) has a Fe:Mn ratio of 0:1 and has two diffraction lines at 2.67 and 1.59 Å, both of which are significantly larger than the *d* values of two-line ferrihydrite.

All five observations of these poorly crystalline, Fe/Mn hydrous oxides show that they hold significant amounts of metals, including Cu, Zn, As, and Pb, that are known to be the most abundant toxic heavy metals in the Clark Fork River Superfund Complex. EDX shows that the $(\text{Cu} + \text{Zn}) : (\text{Fe} + \text{Mn})$ ratio can be as high as 10:100.

The textures of the five observed hydrous oxides are relevant and are discussed below. The samples with the highest Fe/Mn

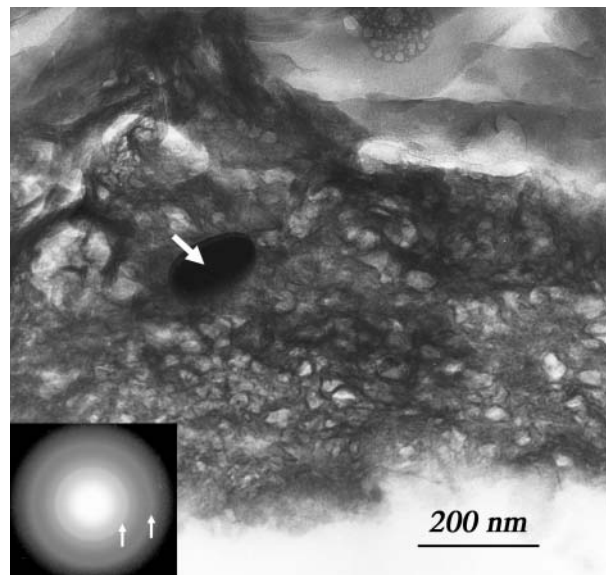


FIGURE 6. TEM image of an example of the vernadite-like mineral with no intermixed ferrihydrite, collected from the riverbed at Kohr's Bend. The arrow in the image points to what may be a bacterial remnant. In the diffraction pattern, the inner and outer arrows point to the diffraction bands at 2.67 and 1.59 Å, respectively. The diffraction band between them is from the epoxy/carbon film holding the specimen.

ratio described above, each exhibiting a two- or six-line ferrihydrite diffraction pattern, show either a mottled or spotted texture with just a few fiber- or sheet-like features (MC-riverbed; Fig. 2; and KB-floodplain1, Fig. 3), or a smooth, even texture (KB-floodplain2; Fig. 4). In contrast, the samples with more Mn show a different texture. One of these samples from KB-floodplain2 (Fig. 5) exhibits a coarsely mottled texture with fine fiber- or sheet-like features running throughout. The all-Mn hydrous oxide from the riverbed at Kohr's Bend (KB-riverbed; Fig. 6) exhibits yet another texture. This sample is relatively coarsely mottled and made up of what seems to be a random array of very thin sheets.

DISCUSSION

The most likely identification of the all-Mn oxide observed from the riverbed at Kohr's Bend (KB-riverbed; Fig. 6) would be the mineral vernadite which is, like ferrihydrite, a poorly crystalline hydrous oxide with exceptionally high surface area (for example, see Post 1999). Although its atomic structure is poorly understood (Manceau and Combes 1988), the structure has been suggested to be similar to that of birnessite, a layered Mn hydrous oxide, except that vernadite is disordered in the layer-stacking direction (e.g., Giovanoli 1980). However, all previously described diffraction patterns of vernadite show two broad diffraction lines at 2.4 to 2.5 Å and 1.4 to 1.5 Å (Post 1999). As mentioned above and listed in Table 1, the mineral in Figure 6 has diffraction lines at 2.67 and 1.59 Å, values that are significantly larger than those of vernadite.

A clue as to a possible explanation of the above observations may be found in the textures of these minerals. TEM images of ferrihydrite are generally mottled or spotted, which results from

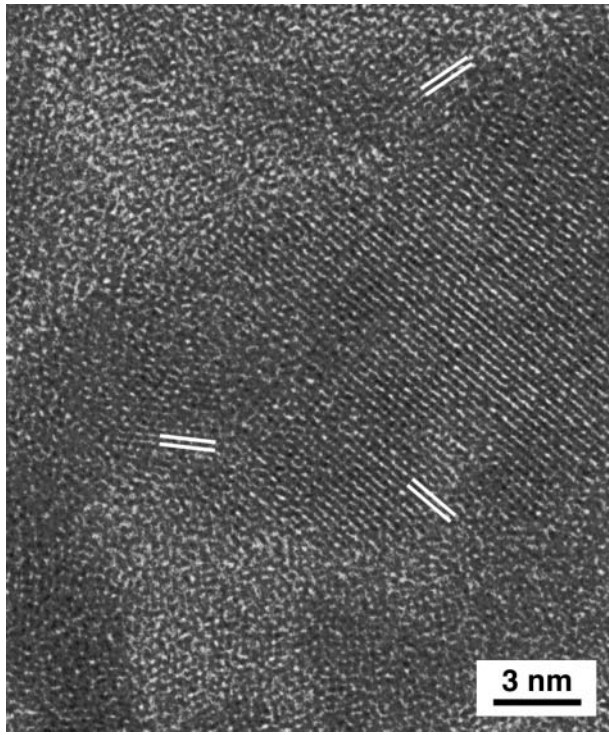


FIGURE 7. High-resolution TEM image of the vernadite-like mineral shown in Figure 6, showing lattice fringes at a spacing of approximately 2.8 Å.

imaging exceptionally small individual particles, on the order of a few nanometers (e.g., Eggleton 1987; Hochella et al. 1999; Janney et al. 2000). The two- and six-line ferrihydrite samples observed in this study have either this texture (Figs. 2 and 3) or have the smooth texture (Fig. 4) that has also been observed in some other examples of ferrihydrite (e.g., Schwertmann and Cornell 1991). Except for a few thin fibers or sheets seen among the ferrihydrite in Figure 2, nothing seems out of the ordinary texturally. However, the hydrous oxides observed here with more Mn, or all-Mn (Figs. 5 and 6) show a very different texture as previously described in the Results section above. These materials have exceptionally fine fibers or sheets throughout, the kind of texture that has been observed before for synthetic random-stacked birnessite, i.e., vernadite (Yang and Wang 2002). It is also critical to note that Manceau and Combes (1988), in their EXAFS study of Fe-containing vernadite, conclusively showed that vernadite has no corner-sharing octahedra and is therefore a sheet manganate. Also, they showed that the Fe incorporated in the mineral has a distinct local environment, separate from the Mn environment, and therefore an Fe-for-Mn substitution in vernadite seems to be ruled out. As a result, Mn and Fe atoms must be clustered separately, resulting in two intimately mixed phases on the nanoscale.

To characterize further the all-Mn hydrous oxide, high-resolution TEM images were taken within the image area shown in Figure 6. Figure 7 shows an example of such a lattice-resolution image. Lattice spacings of about 2.8 Å can be observed in several places in the image, probably corresponding to the 2.7 Å repeat measured in the electron diffraction pattern. By observing the

extent of the fringes, one can determine the size of individual diffracting particles. This and similar images suggest that discrete particles range in size down to only 1.5 nm, explaining the smooth and broad electron diffraction rings observed.

All of the above, put together, provides a likely explanation for the imaging and diffraction observations reported here. The exceptionally fine “fibers” in Figures 2, 3, 5, and 6 are made up of nanoscale vernadite-like mineral grains, although some may be larger sheets that are being seen on edge. The stippled-texture mineral between the fibers is ferrihydrite (Figs. 2, 3, and 5). The more Mn that is present, the more fibers one will see relative to the stippled ferrihydrite texture. Therefore, as observed in Figure 5 (Fe:Mn = 3:2), the sample has a roughly even mixture of fibers and stippled texture. In Figure 6 (Fe:Mn = 0:1), the sample is made up entirely of fibers and possibly sheets lying in all orientations.

The suggestions above are supported by some additional information. The ring diffraction pattern from the mineral with an Fe:Mn ratio of 3:2 (Fig. 5) is noticeably more diffuse than any other diffraction pattern observed in this study. This makes sense, in that one would expect the pattern from a mixture of ferrihydrite and the vernadite-like mineral to show exactly this effect. The inner diffuse diffraction ring is due to the mixing (overlap) of the ferrihydrite line at approximately 2.55 Å and the vernadite-like mineral line at approximately 2.67 Å. The outer diffuse diffraction ring is due to the mixing of the ferrihydrite line at 1.50 Å and the vernadite-like mineral line at 1.59 Å. The *d* values reported in Figure 5 for this mixed material were obtained by measuring from the center of each diffuse ring, and therefore the values in Table 1 are between those reported for each mineral.

It is important to note that the vernadite-like mineral described in this study may not be a simple modification of vernadite itself. Both vernadite and the vernadite-like mineral observed here have only Mn and O as major elements (with only EDX analysis, we cannot comment on H content), and both have two broad, weak diffraction lines. However, the higher and lower *d* values for the vernadite-like mineral are approximately 0.2 and 0.1 Å larger, respectively, relative to values typically reported for vernadite. One possible explanation is the effect of the heavy metals carried by the vernadite-like mineral described here (As, Cu, Pb, Zn; see Table 1); however, neither of the observed *d* values is likely to be from a basal reflection (Post 1999), and these metals would be expected to occupy sites between MnO_6 octahedral sheets (see the structural study of Cu, Pb, and Zn interlayer complexation in birnessite by Manceau et al. 2002). Because more is not known about the vernadite structure, and because we have only found the vernadite-like mineral in sizes suitable for TEM study, it remains impossible to be more specific about their exact relationship.

It is possible to speculate about the nucleation and growth of the vernadite-like mineral. We suspect that the mineral, in the absence of ferrihydrite (Figs. 6 and 7), has a biogenic origin, whereas that intimately mixed with ferrihydrite (Figs. 2, 3, and 5) has an abiotic origin. There is much laboratory and field evidence that indicates the majority of naturally occurring Mn(IV) oxides, like vernadite, are produced by way of Mn-oxidizing bacteria and fungi, even in anaerobic environments (Tebo et al. 2004,

and references therein). Although it is by no means conclusive evidence, the dark area indicated by the arrow in Figure 6 gives an EDX spectrum with an intense carbon line, and this may be the remains of a portion of an organism that was proximal to these manganese hydroxide grains. Note that these samples were not prepared in a way that would preserve biological structures, which were rarely seen in this study. Therefore, the association of these vernadite-like grains with what may be a biological remnant is notable. In contrast, the vernadite-like mineral intimately mixed with the ferrihydrite may have formed because of the surface-catalyzed abiotic oxidation of Mn^{2+}_{aq} by dissolved O_2 in solution. In this case, the reaction starts on ferrihydrite surfaces followed by an autocatalytic reaction whereby Mn^{2+}_{aq} is oxidized directly on the growing vernadite-like mineral. Although the rates of biologically driven Mn oxidation are generally faster than abiotic rates (e.g., Tebo et al. 2004), it has been known for years that certain inorganic surfaces, including iron oxides, are outstanding at promoting Mn oxidation (e.g., Junta and Hochella 1994, and references therein). Further, a recent study has shown that hematite nanoparticles with a mean diameter of 7 nm drive abiotic Mn oxidation up to two orders of magnitude faster than do hematite nanoparticles with a mean diameter of 37 nm (Madden and Hochella 2005). This difference arises because the electronic structure and the surface characteristics change as the grains get smaller and smaller in the nanoregime (Madden and Hochella 2005). Such an accelerated rate could also be envisioned for ferrihydrite, given its typical grain size at the small end of the nanoscale. Clearly, more study is needed in this area.

IMPORTANT IMPLICATIONS

The TEM/EDX observations of samples from a massive acid mine drainage system, the Clark Fork River Superfund Complex in western Montana, U.S.A., provide a direct look at the heavy-metal uptake ability of ferrihydrite and a vernadite-like mineral, even when both are intermixed on the nanoscale. Such intimate association between various Fe and Mn oxides has been described many times before, as for example by Chukhrov et al. (1979) in their classic description of vernadite and Fe-oxide mixtures in marine ferromanganese nodules. However, we are neither aware of vernadite or a vernadite-like mineral having been reported from areas impacted by mining and smelting, nor are we aware of this vernadite-like mineral ever having been reported. Considering how difficult they are to find, and that Mn is not nearly as abundant as Fe, but, like Fe, is generally present in nature and especially in many heavy-metal ore deposits, such Mn oxides possibly are widespread and important in acid mine-drainage environments. Not only do many oxides of Fe and Mn provide enormous surface areas, but these surfaces are active in sorbing transition metals, the extent depending on the surrounding conditions (pH, Eh, fluid composition; for ferrihydrite, see, e.g., Davis and Kent 1990; Cornell and Schwertmann, 1996, and references therein). In particular, the relative reactivity of the oxides of Fe and Mn has been considered for some time (e.g., McKenzie 1980), and it has been recently shown in flow-through experimental studies that Mn oxides with tunnel and layer structures can take up much more heavy metal per external surface area than several common Fe oxides (O'Reilly and Hochella 2003). Specifically, it was determined that birnessite takes up

nearly an order of magnitude more Pb than ferrihydrite at pH 5.5 when normalized to external surface area. Presumably, this is because tunnel- and layer-structured Mn oxides can take up metals on internal sites, which Fe oxides do not have, as well as on external sites. In this study, it is possible to see a similar trend if the uptake of heavy metals on pure ferrihydrite ($Fe_{100}Mn_0$; Fig. 4) and the ferrihydrite/vernadite-like mineral mixture ($Fe_{60}Mn_{40}$; Fig. 5) are compared. Both are from the same sample collected from the floodplain at the Kohr's Bend sampling location, where each was likely exposed to the same amounts of migrating heavy metals. EDX spectra show that the ferrihydrite has less than half the amount of As, Cu, and Pb as found in the mix of ferrihydrite and vernadite-like mineral, and only the latter has sorbed Zn. Therefore, the inference for this mixed sample is that the vernadite-like mineral has taken up dramatically more metal than the associated ferrihydrite. The extraordinary heavy-metal sorptive capability of the vernadite-like phase makes it a promising candidate as a reactive medium in permeable barriers that are used in environmental remediation.

ACKNOWLEDGMENTS

C. Greffé, J. Jambor, and an anonymous reviewer provided constructive reviews that significantly improved this manuscript. Their efforts are greatly appreciated. M.F.H. is grateful for the generosity and support of the Institut für Mineralogie and Interdisciplinary Centre for Electron Microscopy and Microanalysis, Universität Münster, during a sabbatical leave in the Putnis labs. Ulla Heitmann was exceptionally helpful with the TEM sample preparation, and the authors also appreciate the assistance of K. Pollak, H.-W. Meyer, and J.M. Astilleros. Major funding for this work was granted in the form of a Humboldt Research Award from the Alexander von Humboldt Foundation, Bonn, Germany, and also by a sabbatical leave grant from Virginia Tech. Important additional research funding was provided by NSF grant EAR-01-03053 and DOE grant DE-FG02-02ER15326. The experimental facilities at Münster are supported by grants from the Deutsche Forschungsgemeinschaft (DFG).

REFERENCES CITED

- Alpers, C.N. and Blowes, D.W., Eds. (1994) Environmental geochemistry of sulfide oxidation. American Chemical Society Symposium Series 550, 681 pp. Washington, D.C.
- Alpers, C.N., Blowes, D.W., Nordstrom, D.K., and Jambor, J.L. (1994) Secondary minerals and acid mine-water chemistry. In J.L. Jambor and D.W. Blowes, Eds., Environmental Geochemistry of Sulfide Mine-Wastes. Mineralogical Association of Canada Short Course, 22, 247–270. Mineralogical Association of Canada, Nepean, Ontario.
- Banfield, J.F. and Nealson, K.H., Eds. (1997) Geomicrobiology: Interactions Between Microbes and Minerals, vol. 35. Reviews in Mineralogy, Mineralogical Society of America, Washington, D.C.
- Buseck, P.R., Jacob, D.J., Pósfai, M., Li, J., and Anderson, J.R. (2000) Minerals in the air: An environmental perspective. International Geology Review, 42, 577–593.
- Chukhrov, F.V., Gorshkov, A.I., Beresovskaya, V.V., and Sivtsov, A.V. (1979) Contribution to the mineralogy of authigenic manganese phases from marine manganese deposits. Mineralium Deposita, 14, 249–261.
- Cornell, R.M. and Schwertmann, U. (1996) The Iron Oxides. Structure, Properties, Reactions, Occurrence, and Uses. VCH, Weinheim.
- DaRosa, C.D. and Lyons, J.S. (1997) Hardrock mining and water: An overview. In P.M. Hocker, Ed., Golden Dreams, Poisoned Streams, p. 3–24. Mineral Policy Center, Washington, D.C.
- Davis, J.A. and Kent, D.B. (1990) Surface complexation modeling in aqueous geochemistry. In M.F. Hochella Jr. and A.F. White, Eds., Mineral-Water Interface Geochemistry, 23, 177–260. Reviews in Mineralogy, Mineralogical Society of America, Washington, D.C.
- Davis, A., Drexler, J.W., Ruby, M.V., and Nicholson, A. (1993) Micromineralogy of mine wastes in relation to lead bioavailability, Butte, Montana. Environmental Science and Technology, 27, 1415–1425.
- Eggerton, R.A. (1987) Noncrystalline Fe-Si-Al-oxyhydroxides. Clays and Clay Minerals, 35, 29–37.
- Giovanni, R. (1980) Vernadite is random-stacked birnessite. Mineralium Deposita, 15, 251–253.
- Hochella, M.F., Jr. (2002) Sustaining Earth: Thoughts on the present and future roles of mineralogy in environmental science. Mineralogical Magazine, 66, 627–652.

- Hochella, M.F., Jr., Moore, J.N., Golla, U., and Putnis, A. (1999) A TEM study of samples from acid mine drainage systems: Metal–mineral association with implications for transport. *Geochimica et Cosmochimica Acta*, 63, 3395–3406.
- Hochella, M.F., Jr., Moore, J.N., Putnis, C., Putnis, A., Kasama, T., and Eberl, D. (2005) Direct observation of toxic metal–mineral association from the Clark Fork River Superfund Complex: Implications for metal transport and bioavailability. *Geochimica et Cosmochimica Acta*, in press.
- Holmström, H. and Öhlander, B. (2001) Layers rich in Fe- and Mn-oxyhydroxides formed at the tailings-pond water interface, a possible trap for trace metals in flooded mine tailings. *Journal of Geochemical Exploration*, 74, 189–203.
- Hudson-Edwards, K.A., Macklin, M.G., Curtis, C.D., and Vaughan, D.J. (1996) Processes of formation and distribution of Pb-, Zn-, Cd-, and Cu-bearing minerals in the Tyn Basin, Northwest England: Implications for metal-contaminated river systems. *Environmental Science and Technology*, 30, 72–80.
- Jambor, J.L. and Blowes, D.W., Eds. (1994) Environmental Geochemistry of Sulfide Mine-Wastes. Mineralogical Association of Canada Short Course, 22, 438 pp. Mineralogical Association of Canada, Nepean, Ontario.
- Jambor, J.L. and Blowes, D.W. (1998) Theory and applications of mineralogy in environmental studies of sulfide-bearing mine wastes. In L.J. Cabri and D.J. Vaughan, Eds., *Modern Approaches to Ore and Environmental Mineralogy*. Mineralogical Association of Canada Short Course, 27, 367–401. Mineralogical Association of Canada, Nepean, Ontario.
- Jambor, J.L., Blowes, D.W., and Ritchie, A.I.M., Eds. (2003) Environmental Aspects of Mine Wastes. Mineralogical Association of Canada Short Course, 31, 430 pp. Mineralogical Association of Canada, Nepean, Ontario.
- Janney, D.E., Cowley, J.M., and Buseck, P.R. (2000) Transmission electron microscopy of synthetic 2- and 6-line ferrihydrite. *Clays and Clay Minerals*, 48, 111–119.
- Junta, J.L. and Hochella, M.F. Jr. (1994) Manganese (II) oxidation at mineral surfaces: A microscopic and spectroscopic study. *Geochimica et Cosmochimica Acta*, 58, 4895–4999.
- Lind, C.J. and Hem, J.D. (1993) Manganese minerals and associated fine particulates in the streambed of Pinol Creek, Arizona, U.S.A.: A mining-related acid drainage problem. *Applied Geochemistry*, 8, 67–80.
- Madden, A. and Hochella, M.F. Jr. (2005) A test of geochemical reactivity as a function of mineral size: Manganese oxidation promoted by hematite nanoparticles. *Geochimica et Cosmochimica Acta*, in press.
- Manceau, A. and Combes, J.M. (1988) Structure of Mn and Fe oxides and oxyhydroxides: A topological approach by EXAFS. *Physics and Chemistry of Minerals*, 15, 283–295.
- Manceau, A., Lanson, B., and Drits, V.A. (2002) Structure of heavy-metal sorbed birnessite: Part III. Results from powder and polarized extended X-ray absorption fine structure spectroscopy. *Geochimica et Cosmochimica Acta*, 66, 2639–2663.
- McKenzie, R.M. (1980) The adsorption of lead and other heavy metals on oxides of manganese and iron. *Australian Journal of Soil Research*, 18, 61–73.
- Moore, J.N. and Luoma, S.N. (1990) Hazardous wastes from large-scale metal extraction: A case study. *Environmental Science and Technology*, 24, 1278–1285.
- O'Reilly, S.E. and Hochella, M.F. Jr. (2003) Lead sorption efficiencies of natural and synthetic Mn and Fe-oxides. *Geochimica et Cosmochimica Acta*, 67, 4471–4487.
- Post, J.E. (1999) Manganese oxide minerals: Crystal structures and economic and environmental significance. *Proceedings of the National Academy of Sciences U.S.A.*, 96, 3447–3454.
- Schwertmann, U. and Cornell, R.M. (1991) *Iron Oxides in the Laboratory*, 137 pp. VCH, Weinheim.
- Schwertmann, U., Bigham, J.M., and Murad, E. (1995) The first occurrence of schwertmannite in a natural stream environment. *European Journal of Mineralogy*, 7, 547–552.
- Tebo, B.M., Barger, J.R., Clement, B., Dick, G., Murray, K.J., Parker, D., Verity, R., and Webb, S. (2004) Biogenic manganese oxides: Properties and mechanisms of formation. *Annual Reviews of Earth and Planetary Sciences*, 32, 287–328.
- Williams, D.B. and Carter, C.B. (1996) *Transmission Electron Microscopy, A Textbook for Materials Science*, 990 pp. Plenum Press, New York.
- Yang, D.S. and Wang, M.K. (2002) Syntheses and characterization of birnessite by oxidizing pyrochroite in alkaline conditions. *Clays and Clay Minerals*, 50, 63–69.

MANUSCRIPT RECEIVED DECEMBER 28, 2003

MANUSCRIPT ACCEPTED OCTOBER 16, 2004

MANUSCRIPT HANDLED BY JOHN JAMBOR